Journal of Materials Chemistry A

Accepted Manuscript

ROYAL SOCIETY OF CHEMISTRY

www.rsc.org/materialsA

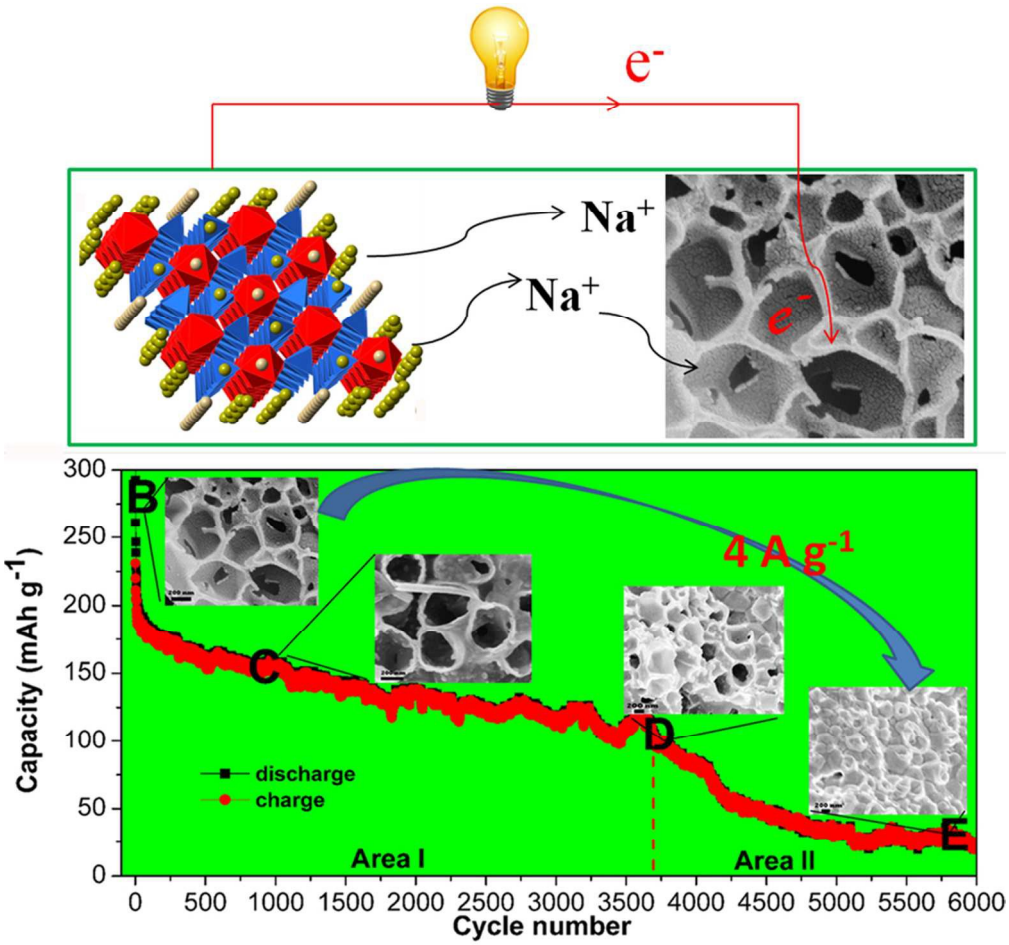

A three-dimensional (3D) hard carbon matrix (3DHCM) derived from sodium polyacrylate precursor was achieved, delivering a superior-rate performance and ultralong cycle life performance, and a sodium-ion full cell property
39x37mm (600 x 600 DPI)

Cite this: DOI: 10.1039/c0xx00000x

www.rsc.org/xxxxxx

ARTICLE TYPE

Three-dimensional hard carbon matrix for sodium-ion battery anode with superior-rate performance and ultralong cycle life†

Zhengqiu Yuan,*[a,b] Lulu Si,[b] and Xiaobo Zhu[b]

Received (in XXX, XXX) Xth XXXXXXXXX 20XX, Accepted Xth XXXXXXXXX 20XX

DOI: 10.1039/b000000x

Taking advantage of the sodium polyacrylate, composed of interlaced carbon chains and inorganic functional groups (-COONa) uniformly grafting onto the carbon chains, a three-dimensional hard carbon matrix (3DHCM) is obtained. The resultant materials are composed of three-dimensional macroporous interconnected networks of carbon nanosheets (thickness, 5-30 nm). The 3DHCM is studied as an anode material for sodium-ion batteries. The unique three-dimensional porous structure results in a high initial charge capacity of 341 mAh g^{-1}, stable cycling capacity of 232.8 mAh g^{-1} (after 100cycles, 50 mA g^{-1}), and superior-rate performance (stable capacities of 210, 197, 128 and 112 mAh g^{-1} at 200, 500, 5000, 8000 mA g^{-1}, respectively) and ultralong cycle life (116 mA h g^{-1} at 4 A g^{-1} after 3,000cycles). At the same time, the trend of the sloping capacity percentage in total discharge increasing is observed. More obvious "graphic" domains with larger interplanar spacing (~0.46 nm) are produced in electrochemical cycles and detected by ex-situ HRTEM, further confirming that the first higher-voltage region (above 0.1 V) should be attributed to the sodium insertion between the parallel graphene layers in the hard carbon. We also find that the electrolyte (1 M $NaClO_4$ in PC) is severely decomposing on the electrode/electrolyte interface in deep electrochemical cycles (6000 cycles), resulting in the deterioration of the electrode and fast capacity fading. Furthermore, a room-temperature sodium-ion full cell is constructed using 3DHCM as anode and $Na_3V_2(PO_4)_3$/C as cathode, (-) 3DHCM ‖ 1M $NaClO_4$ in PC ‖ $Na_3V_2(PO_4)_3$/C (+), delivering the discharge capacity of 90 mAh g^{-1} at the current density of 500 mA g^{-1}. We believe that our findings will be helpful in speeding up the development of room-temperature high-rate, long life and low cost sodium-ion batteries for large-scale energy storage system, and even alternative to lithium-ion batteries.

Intruduction

Clean energy technologies are of importance to preserve the global sustainability by addressing energy shortages and environmental issues. Due to high energy density, lithium-ion batteries (LIBs) are currently prior technology of choice to develop renewable energy technology and in particular electric vehicles (EVs). With the success of Tesla Model S all over the world, EVs are to gain a significant share of future automobile markets. Therefore, the lithium-ion battery production and the proportional demand of the lithium must grow and perhaps unsustainably because the abundance of lithium in the earth crust is as low as 0.0065%. So there is growing concern about the increasing cost and uneven geological distribution of lithium resource. In the context, intensive efforts have been devoted to exploring new reliable energy technology with low cost, long-life time and high-efficiency.[1]

In sharp contrast to lithium, sodium resources are beyond doubt practically inexhaustible, ubiquitous, and environmentally benign, and these factors have stimulated worldwide interest in room-temperature sodium-ion batteries (SIBs) as a low cost electrical energy storage technology, particularly with regard to large-scale applications, and possible alternative to LIBs.[2-5] Given the similarity between Li and Na ion batteries, many SIBs cathode materials have been investigated, such as Na_xCoO_2[6], $Na_{0.44}MnO_2$[7], $NaCrO_2$[8], NaV_6O_{15}[9], $Na_{1-x}Ni_{0.5}Mn_{0.5}O_2$[10], $Na_{2/3}Co_{2/3}Mn_{1/3}O_2$[11], $NaNi_{1/3}Mn_{1/3}Co_{1/3}O_2$[12], $NaFePO_4$[13], $NaFeSO_4F$[14], $NaV_{1-x}Cr_xPO_4F$[15], $Na_3V_2(PO_4)_3$[16] and $Na_{0.67}Mn_{1-x}Mg_xO_2$ ($0 \leq x \leq 0.2$)[17]. However, the ionic radius of Na^+ (102 nm) is larger than that of Li^+ (76 nm), resulting in a poorer kinetics for Na^+ de/insertion reaction, fast capacity fading during cycling and lack of appropriate electrode materials, which seriously restricts the further development of SIBs.[2] Fortunately, it has been making a breakthrough on study of high-rate performance and cycling stability of $Na_3V_2(PO_4)_3$ for SIB cathode. Porous $Na_3V_2(PO_4)_3$/C was capable of delivering 82 mAh g^{-1} for 3,500 cycles at 20 C and nearly 50% of the initial capacity was retained after 30,000 cycles at 40 C.[18] Recently, Y. Yu et al. developed an ultrafast Na-storage carbon-coated $Na_3V_2(PO_4)_3$, delivering high capacity of 91 mAh g^{-1} at 50 C.[19] Compared to the success of the cathode materials for SIBs, the study of the anode moves slowly, especially high-rate performance and cycling stability. It has been widely accepted that only a small amount of sodium can intercalate into graphite.[20] Inspired by LIB-anode analogues,

substantial anode materials have been evaluated for Na storage, with less obvious choices being available for the SIB anode. Several oxides, such as $Na_2Ti_3O_7$, and alloys (Sn or Sb) have been investigated as high storage capacity, but would not be suitable for long life batteries due to large volume change during sodium insertion and extraction, which is undesirable to the structural stability.[21-24] Recently, Wang et al. reported a zero-strain layered metal oxide P2-$Na_{0.66}[Li_{0.22}Ti_{0.78}]O_2$ as anode electrode, exhibiting an average storage voltage of 0.75V, a practical usable capacity of about 100 mAh g^{-1}.[25] However, the material P2-$Na_{0.66}[Li_{0.22}Ti_{0.78}]O_2$ contains the expensive Li source and its capacity is only 50 mAh g^{-1} after 1,200 cycles at 2C.[25] Among the known anode materials, hard carbon shows the best sodium storage performance in terms of high storage capacity, good cycling, and especially the very low cost.

The electrochemical insertion of sodium ions into carbon as first studied by Doeff et al., was reported to generate a reversible capacity of about 85 mA h g^{-1}.[26] Subsequent works on various types of carbonaceous materials have demonstrated that disordered carbon appears to be the most suitable anode material for SIBs. The highest reversible sodium capacity of 300 mA h g^{-1} was achieved for hard carbons derived from pyrolyzed glucose.[27] However, some fatal problems of the hard carbon used in sodium-ion batteries must be mentioned. First, the cyclability and rate capability in previous studies are insufficient, whilst the majority of these studies were also performed under either very low current density or high temperatures. Second, most of the capacity is located at the voltage below 0.1 V, which is too close to the sodium plating voltage, resulting in potential safety concerns, especially at fast charging rates or overcharging. More recently nitrogen doped technology,[28] electrolyte optimizing,[29] and hollow carbon[30, 31] have been adopted to effectively improve the cyclability and rate capability of hard carbon. Carbon nanosheet frameworks derived from peat moss can deliver stable capacity of 203 mA h g^{-1} after 210 cycles at 500 mA g^{-1}.[32] Recently, Y. Yu et al. prepared porous carbon nanofibers with a reversible capacity of 140 mA h g^{-1} after 1,000 cycles at 500 mA g^{-1} (2C).[33] However, the improved hard carbons are still far from the ideal operation conditions to make a serious market and application impact for SIBs. Compared to the superior-rate performance of $Na_3V_2(PO_4)_3$ cathode (e. g., 50 C), the present performance of the sodium storage of hard carbon as anode is imbalanced and need to be further improved urgently, in particular the high-rate performance, cycle life and safety issue. As Okada et al. suggested, the first higher-voltage region (above 0.1 V) should be attributed to the sodium insertion between the parallel graphene layers in the hard carbon, while the second lower-voltage region (below 0.1 V) should be attributed to the sodium insertion into the micropores of hard carbon, and therefore it is logical to increase the part of the parallel graphene layers in hard carbon to obtain more capacity located above 0.1 V.[34] A survey of the existing literature on carbons with optimum energy storage attributes shows that it is essential to couple the intrinsic structure of the precursor with tailored carbonization/ activation treatment.[32, 35, 36] In addition, hierarchical porous nanostructure enabling short transport length for ions is favorable for kinetics of Na^+ de/insertion reaction, resulting in high-rate performance. [33]

Unlike traditional polymer, sodium polyacrylate not only has the long and interlaced carbon chains, but it also has inorganic functional groups (-COONa) uniformly grafting onto the carbon chains. The special structure would make it difficult to graphitize the majority of the material even at high carbonization temperatures[37] and porosity by releasing CO_2 and producing water-soluble substances. In this work, we take the advantage of the special molecular structure of sodium polyacrylate. Through a facile synthesis process of carbonization and possible self-activation, sodium polyacrylate is converted into 3-D hard carbon matrix (3DHCM) with high rate behavior and ultralong cycle life for SIB anode. After 3,000 cycles, the reversible Na-storage capacity of 116 mA h g^{-1} can still be achieved at superior rate 4 A g^{-1} (20 C, 1C= 200 mA g^{-1}). To the best of our knowledge, this high rate behavior is unprecedented for a nonaqueous room temperature SIB anode. Furthermore, we study the morphology change of the carbon matrix during electrochemical cycles for finding the source of superior cycle stability. Lastly, a sodium-ion full cell is also demonstrated using 3DHCM as anode and $Na_3V_2(PO_4)_3$/C as cathode.

Methods

Material Synthesis

Sodium polyacrylate (MW≥ 30 million, SCRC30213370) was purchased from Sinopharm, China. For the pyrolysis carbonization process, typically gram-scale sodium polyacrylate was loaded in a tubular furnace and carbonized at the temperature of 1100 ℃ for 10 h with N_2 flow of 100 sccm min^{-1}. The heating rate was 5 min^{-1}. When exposed in air, the finally formed bulk-like carbonization product gave off a lot of heat. The cooled carbonization product was carefully washed by deionized water, till to PH= 7~8. After drying at 100 ℃ over night in a vacuum oven, the three-dimensional hard carbon matrix was achieved.

Material Characterization

X-ray powder diffraction (XRD) measurements were determined by a Bruker D8 advanced X-ray diffractmeter. The scanning electron microscopy (SEM) images were taken by using a field-emitting scanning electron microscope (FESEM, JEOL-JSM-6700F). The transmission electron microscopy (TEM) images and high-resolution transmission electron microscopy (HRTEM) images were taken on a JEOL-2010 transmission electron microscope with an accelerating voltage of 200 kV. Raman spectrum was carried out on a JY LABRAM-HR confocal laser micro-Raman spectrometer using Ar^+ laser excitation with a wavelength of 514.5 nm.

Electrochemical Test.

Electrochemical tests were carried out using coin cells CR2016. The slurry of 80% active materials, 10% carbon black (Super-P), and 10% poly(vinlylidenedifluoride) (PVDF) in N-methylpyrrolidone (NMP) was coated on copper foil using a doctor blade and then dried at 110 ℃ over night in a vacuum oven, resulting in electrodes with a mass loading of about 1 mg cm^{-2}. Na metal was used as counter electrode and separated from the working electrodes with glass fiber (Whatman, GF/B). The electrolyte was 1 M $NaClO_4$ dissolved in propylene carbonate (PC). Cyclic voltammetry measurements were conducted on

Tianjin LK2005A system. The charge-discharge measurements were performed using LAND CT 2001A (Wuhan, China). A sodium-ion full cell was constructed using 3DHCM as the negative electrode and $Na_3V_2(PO_4)_3$/C as the positive electrode in a CR2016 coin-type cell. The $Na_3V_2(PO_4)_3$/C electrode was prepared according to Ref. 47. The weight ratio of the two electrodes (negative/positive) was 1:1.9. The ratio value is not the optimal one. The full cell system was (-) 3DHCM ‖ 1M $NaClO_4$ in PC ‖ $Na_3V_2(PO_4)_3$/C (+) and two electrodes were separated by glass fiber. The full cell was charged and discharged between the voltage ranges of 0.5–3.5V at the current density of 500 mA g^{-1} (based on 3DHCM mass).

Results and Discussion

Synthesis and characterization of 3DHCM

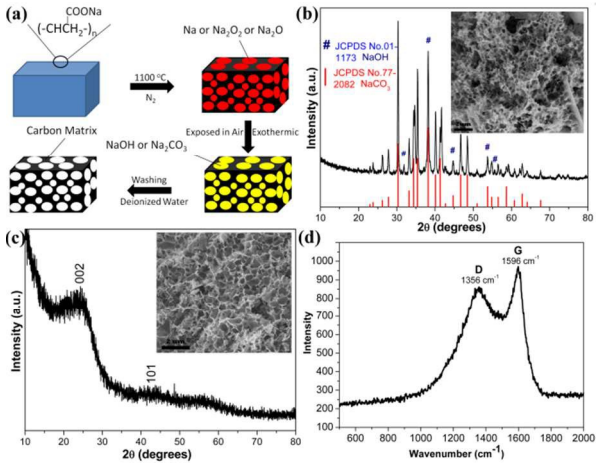

Figure 1 (a) Schematic illustration of the synthesis process for 3-D hard carbon matrix. (b) X-ray diffraction (XRD) pattern of the cooled carbonization product exposed in air. (c) X-ray diffraction (XRD) pattern of the 3-D hard carbon matrix (3DHCM). (d) Raman spectrum of the 3DHCM.

Figure 1a schematically illustrates the experimental process. The sodium polyacrylate precursor was first carbonized at 1100 ºC under inert atmosphere (N_2) for 10 h. During the pyrolysis process, the long and interlaced organic carbon chains were converted into inorganic carbon. At the same time, inorganic functional groups (-COONa) may decomposed into CO_2, Na_2O, Na_2O_2 and even metal sodium (Na) due to the spontaneous combustion of the newly formed carbonization product in water. On the one hand, Na_2O decompose into Na_2O_2 and Na above 400 ºC; on the other hand, the sodium may be evolved during the reaction between carbon and sodium oxides.[38] When exposed in air, the newly formed bulk-like carbonization product gave off a lot of heat because the embedded sodium or sodium oxides adsorbed moisture and CO_2 in air and converted into NaOH and $NaCO_3$ with exothermic reactions. Figure 1b shows the XRD pattern of the cooled bulk-like carbonization product in air. The diffraction peaks correspond to crystal $NaCO_3$ and NaOH, and are labeled respectively in Figure 1b. No obvious diffraction peaks can be ascribed to carbon. Insert of Figure 1b displays the scanning electron microscope (SEM) image of the cooled bulk-like carbonization product, showing the corals-like morphology. After water washing, the inorganic substances ($NaCO_3$ and NaOH) can be removed completely from the carbonization product, leaving lots of pores in the final carbon product. The SEM image of the carbon product is displayed in the insert of Figure 1c. Lots of pores with the size of hundred nanometers uniformly distribute in the interconnected three-dimensional (3-D) hard carbon matrix (3DHCM), which is favorable for electrolyte access to the active materials without the electrical charge transport limitation. XRD pattern of the 3DHCM is displayed in Figure 1c. The wide diffraction peaks observed at 2θ values of 23.42° and 43.29°, correspond to (002) diffraction of the graphitic layer structure and the (101) diffraction of graphite, respectively. The interlayer spacing of d_{002} was calculated to be 0.379 nm, which is wider than that of the graphite (0.335 nm). Considering the larger diameter of sodium ions, the large free space between graphene layers should be favorable for the reversible storage of sodium ions.[31] The Raman spectrum of the 3DHCM (Figure 1d) exhibits two pronounced shifts, the peak located at ~1596 cm^{-1} is named as G-band and ascribed to the E_{2g} graphitic mode, while the D-band peak at ~1356 cm^{-1} corresponds to a defect-induced mode.[39] The intensity ratio (R) between the D and G band (R = ID/IG) is an index of the disorder degree of the carbon. The R value for the 3DHCM is 0.89, indicating a highly disordered structure.[40]

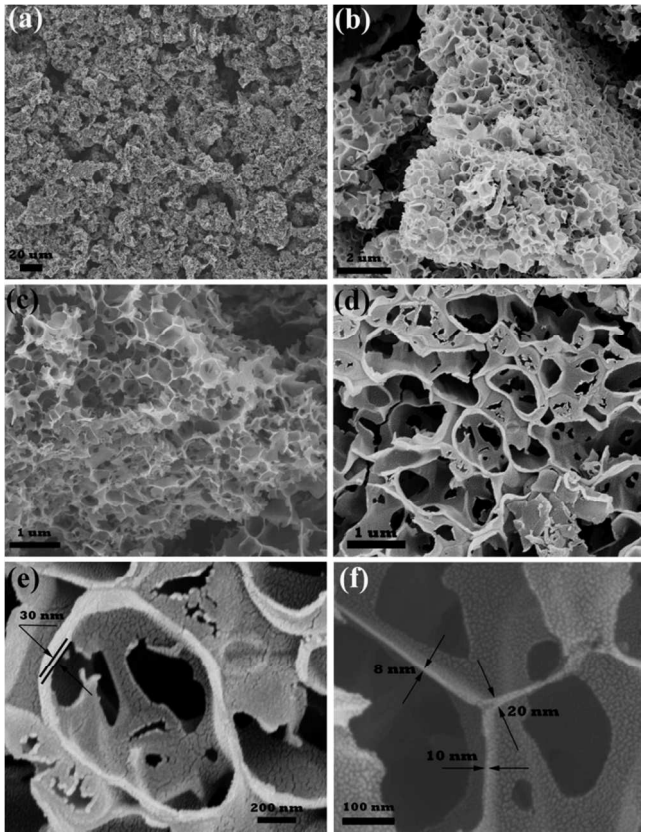

Figure 2 (a) Low magnification SEM image of the 3DHCM. (b-c) Medium magnification SEM images of the 3DHCM. (d) Higher magnification SEM image highlighting the hollow macroporous architecture of 3DHCM. (e-f) The partial enlarged high-resolution images of the wall of the macropore and the connected part between the pores, respectively.

After grinding, the previous centimeter level 3DHCM bulk breaks up into irregularly shaped carbon particles with the dimensions ranging from 10 to 30 μm (Figure 2a). Figure 2b and 2c show the medium images of 3DHCM, lots of macropores

uniformly distribute in the carbon particle. According to the SEM image (Figure 2d), each carbon particle displays a hollow 3-D architecture with linked macropores. The unique 3-D open structure of the 3DHCM could facilitate the electrolyte penetration and ion diffusion. Figure 2e and 2f display the wall of the macropore and the connected part between the pores, respectively. The thicknesses of the wall of the macropore and the connected part between the pores are 5-30 nm in dimensions. The resultant distances of sodium ion diffusion are at the maximum of half of those thicknesses (2.5-15 nm) because of electrolyte contacting on the both sides of the pores. The short diffusion distances are favorable for fast sodium insertion/extraction. As will be demonstrated, the intrinsic macroscopic openness of 3DHCM composed of very thin interconnected carbon nanosheets is one essential feature for optimum material utilization during the electrochemical sodium insertion/extraction, especially the high-rate performance.

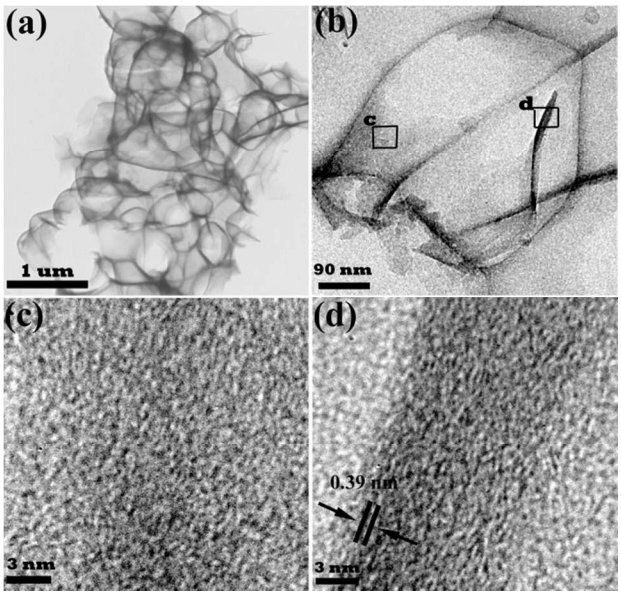

Figure 3 (a-b) TEM micrographs of the 3DHCM. (c-d) HRTEM micrographs of 3DHCM, respectively, squared in (b).

The transmission electron microscopy (TEM) and HRTEM micrographs (Figure 3) confirm that the 3DHCM consist of highly disordered and interconnected carbon sheets and its macroporous feature. From TEM image (Figure 3a and 3b), the interconnected parts between the neighboring macropores can be clearly observed and distribute uniformly and continuously. The interconnected structure strengthens the internal electronic continuous conduction. Figure 3c shows the HRTEM micrograph of the macropore wall, indicating highly disordered structure (close to amorphous) without any "graphitic" domains. Interestingly, the connected parts between the neighboring macropores are more ordered than the macropore walls. According to the HRTEM image of the selected area of the connected part (Figure 3d), some fuzzy "graphitic" domains can be observed, which are formed by few-layer stacked graphene sheets. The average spacing between the graphene layers is approximately 0.39 nm, which is consistent with the XRD value of d_{002}. Such open structures are known to allow for facile sodium ion insertion/extraction between the graphene layers.[31] The voltage of the sodium insertion between the parallel graphene layers locates at safe region (1.2-0.1 V). [29, 34]

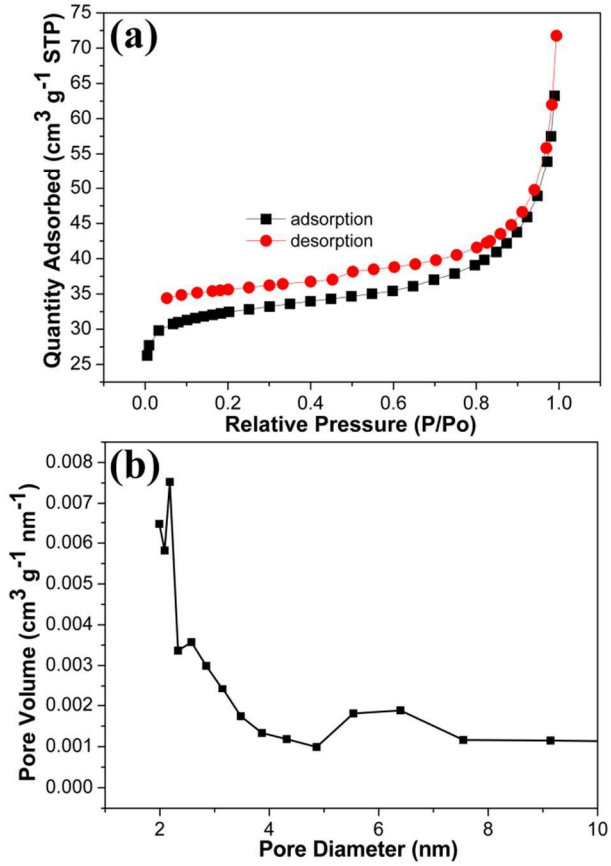

Figure 4 (a) Nitrogen adsorption-desorption isotherms of 3DHCM. (b) Pore size distribution.

The 3DHCM shows HRTEM contrast consistent with what is typically reported for microporous and mesoporous carbons.[32, 41] To further examine the surface and characterize the pore size of the 3DHCM, N_2 adsorption–desorption isotherms were measured. Figure 4a shows nitrogen adsorption-desorption isotherms of 3DHCM, indicating a type IV isotherms, with a high Brunauer–Emmett–Teller (BET) surface area of 108.9 $m^2 g^{-1}$. The pore size distribution is displayed in Figure 4b. The 3DHCM displays a pore volume of 0.083 $cm^3 g^{-1}$, and possesses mesopores (peaks at 2.1, 2.5 and 6.0 nm), corroborating the HRTEM (Figure 3c and 3d) results.

Electrochemical performance

To investigate the electrochemical energy storage properties of the 3DHCM, we performed cyclic voltammetry (CV) and galvanostatic discharge/charge cycling by using a half-cell with sodium metal. Figure 5a shows representative CV curves of the 3DHCM electrode tested between 0 and 3 V at a scanning rate of 0.2 mV s^{-1}. The sharp reduction peak at 0.3 V during the cathodic process in the first CV scan is generally ascribed to the electrolyte decomposition and the formation of a solid electrolyte interphase (SEI) layer on the carbon surface, as compared to the lithium-ion and sodium-ion system.[30, 31, 41] This peak could still be observed in the second CV scan, indicating the SEI layer was further improved. After the third scan, the 0.3 V peak disappeared, which can be attributed to isolation of the active material from the electrolyte due to the dense SEI layer formed

on the surface of the anode in the front two discharges. At the low voltage region, there is a sharp cathodic peak near 0 V and a counterpart anodic peak at 0.20 V, resembling the CV behavior of lithium insertion/extraction in graphite.[42] Besides the sharp peaks, there is also a pair of weak ones over a wide voltage region (0.2-1.2 V) in both the cathodic and the anodic portions.

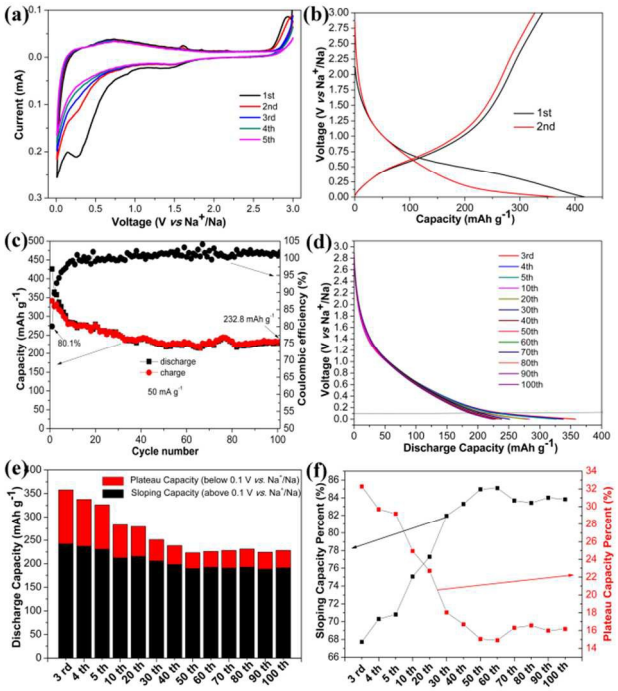

Figure 5 (a) Cyclic voltammogram (CV) of 3DHCM electrode between 0 and 3 V at a scanning rate of 0.2 mV s^{-1}. (b) Galvanostatic discharge/charge curves of 3DHCM electrode at current density of 50 mAh g^{-1}. (c) Cycle performances of 3DHCM electrode at a current density of 50 mA g^{-1}. (d) Discharge curves of 3rd, 4th, 5th, 10th, 20th, 30th, 40th, 50th, 60th, 70th, 80th, 90th, 100th cycles. (e) Summary of capacity potential distribution of different cycles. (f) Trend of sloping capacity and plateau capacity percentage in whole one cycle discharge capacity with the cycle number increasing.

Figure 5b shows the front two discharge-charge profiles of the 3DHCM electrode. The first discharge-charge cycle reveals the initial discharge and charge capacities to be 426 and 341 mAh g^{-1}, respectively, at a current density of 50 mA g^{-1}. The formation of SEI and any irreversible insertion of Na into the carbon structure are the main reasons for the initial irreversible capacity loss (85 mAh g^{-1}), coinciding with the results from the CV observations. In the subsequent cycles, the 3DHCM electrode displays obvious sloping discharge curves and a plateau below 0.1 V, corresponding to the cathodic peaks observed in CV curves. For instance, the sloping discharge capacity and plateau capacity are 242.3 and 115.5 mAh g^{-1}, respectively, in the third discharge. Results reported earlier have confirmed that the sloping voltage profile can be ascribed to the insertion of sodium between graphene layers, whilst sodium insertion into nanopores takes place at the lowest potentials (called "point I").[31, 34, 41-44] However, Li and Mitlin's recent experimental results were completely opposite of that the low voltage plateau was based on filling of pores by Na metal.[32] At the same time, they also found that the fraction of the total capacity associated with the plateau below 0.1 V increased with the ordering of their carbon materials increasing, which may be explained by arguing that more ordered domains (disordered graphene layers) would provide Na insertion sites that were more energetically equivalent and hence leaded to progressively flatter plateaus (called "point II").[32] Which of the two opposite views is more close to the nature of hard carbon storaging sodium? The analysis of our data about the sloping discharge capacity and plateau capacity is discussed below.

Figure 5c shows the cycling capacity retention performance of the 3DHCM at 50 mA g^{-1}. The reversible capacities of the front cycles are gradually decaying. Specifically, the electrode retains a high reversible capacity of 232.8 mAh g^{-1} after 100 cycles. This cycling performance may be considered one of the best reports, since there are few reports of carbonaceous materials displaying over 230 mAh g^{-1} of stable capacity as a SIB anode.[33, 41] In addition, the initial Coulombic efficiency (CE) is as high as 80.1%, which is the best one in the reported literatures. After the first cycle, the CE increase dramatically upon cycling, reaching 100% nearly after 10 cycles (Figure 5c). Figure 5d shows the discharge curves of 3rd, 4th, 5th, 10th, 20th, 30th, 40th, 50th, 60th, 70th, 80th, 90th, 100th cycles, respectively, at 50 mA g^{-1} between 0 and 3 V. The obvious sloping part and plateau one can be observed. It's worth noting that the plateau part (below 0.1 V) was decreasing gradually with the cycle number increasing. This trend is summarized in histogram shown in Figure 5e, where the fraction of the total discharge capacity associated with the plateau below 0.1 V decreases with the cycle increasing. Figure 5f displays the sloping and plateau capacity percentage in total discharge in each cycle, indicating the trend digitally. At the same time, dozens of half-cells gave the same trend at the identical testing condition. If the "point I" is correct, the units of graphitic microcrystallites are increasing in the electrochemical cycles because the related sloping capacity percentage (safe area) is increasing with the cycles increasing, or/and the nanopores are decreasing, as shown in Figure 5f.

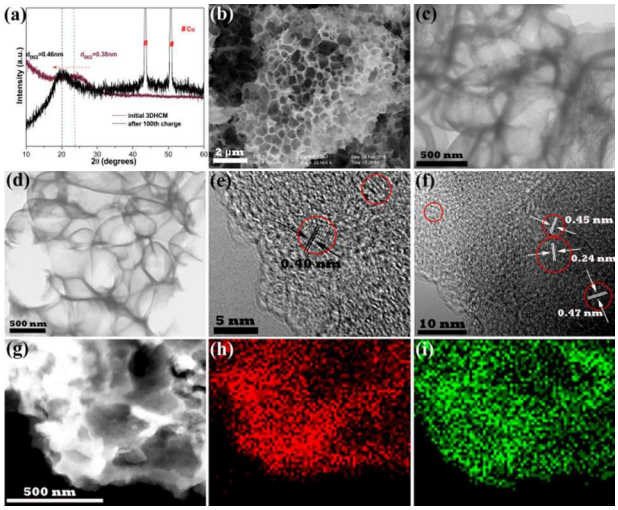

Figure 6 (a) XRD patterns of initial 3DHCM and the electrode after 100th charge. (b, c) SEM and TEM images of electrode material after 100th charge, respectively. (d) TEM image of initial 3DHCM. (e, f) HRTEM images of electrode material after 100th charge. (g) STEM image of the electrode after 100th charge. (h, i) Carbon (red) and sodium (green) elemental mapping images of the electrode after 100th charge, respectively.

To elucidate the trend of the sloping capacity percentage increasing in total discharge, the ex-situ XRD, SEM, TEM and HRTEM characterizations were performed on the cycled electrode at 50 mA h^{-1} between 0 and 3 V (ended at 100th

charge). Figure 6a shows the XRD pattern of the 3DHCM electrode after 100th charge, indicating that intergraphene layer spacing of d_{002} shifts toward higher value (from 0.38 to 0.45 nm) after 100 discharge-charge cycles maybe due to the irreversible sodium-ion insertion. From the SEM of the cycled electrode (Figure 6b), the 3-D structure of the active material can be well preserved, revealing a good stability of the structure in electrochemical cycling. Additionally, TEM images of the electrode after 100th charge (Figure 6c) and (Figure 6d) before reveal that a uniform SEI film was generated on the surface of the electrode and in the macropores, consistent with elemental mapping observations (Figure g-i). Compared to highly disordered structure without any obvious "graphitic" domains (Figure 3c and 3d), more obvious "graphitic" domains can be observed in the HRTEM images of the cycled electrode (Figure 6e and 6f) with the interlayer spacings of 0.40, 0.45 and 0.47 nm, respectively. The larger interlayers space is more conducive to the sodium-ion insertion/extraction. With the obvious "graphitic" domains increasing, the sloping capacity percentage is increasing in total discharge, further indicating that our experimental results confirm to above "point I".

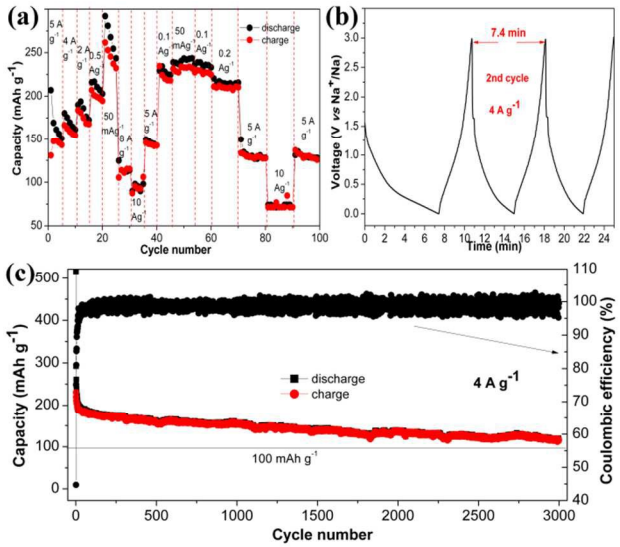

Figure 7 (a) Rate performance of the 3DHCM electrode at different current densities. (b) The voltage-time curves in front three cycles at 4 A g^{-1}. (c) Cycle performance of the 3DHCM electrode the current density of ranging from 0 to 3 V at the current density of 4 A g^{-1}.

To better understand the advantage of using 3DHCM in SIBs, the rate performance of 3DHCM electrode was investigated (Figure 7a). The electrode was firstly cycled at high current densities 5, 4, 2 and 0.5 A g^{-1}, respectively. In front cycles, the reversible capacities are gradually decaying. At 50 mA g^{-1}, the stable reversible capacity of 230 mAh g^{-1} can be obtained. Interestingly, even at very high current densities of 5 and 10 A g^{-1}, reversible capacities of 128 and 72 mAh g^{-1} can still be delivered, respectively. Thus, the electrode exhibits a high rate performance even at very fast sodium ions insertion/extraction speeds. Figure 7b and 7c show the cycle performance of the 3DHCM electrode at the current density of 4 A g^{-1} between 0 and 3 V. Except the first cycle, the time of the discharge-charge cycles are all below 7.4 min (only 3.2 min to charge). At the 1st, 100th, 500th, 1,000th, 1,500th and 2,000th charge, the reversible capacities are

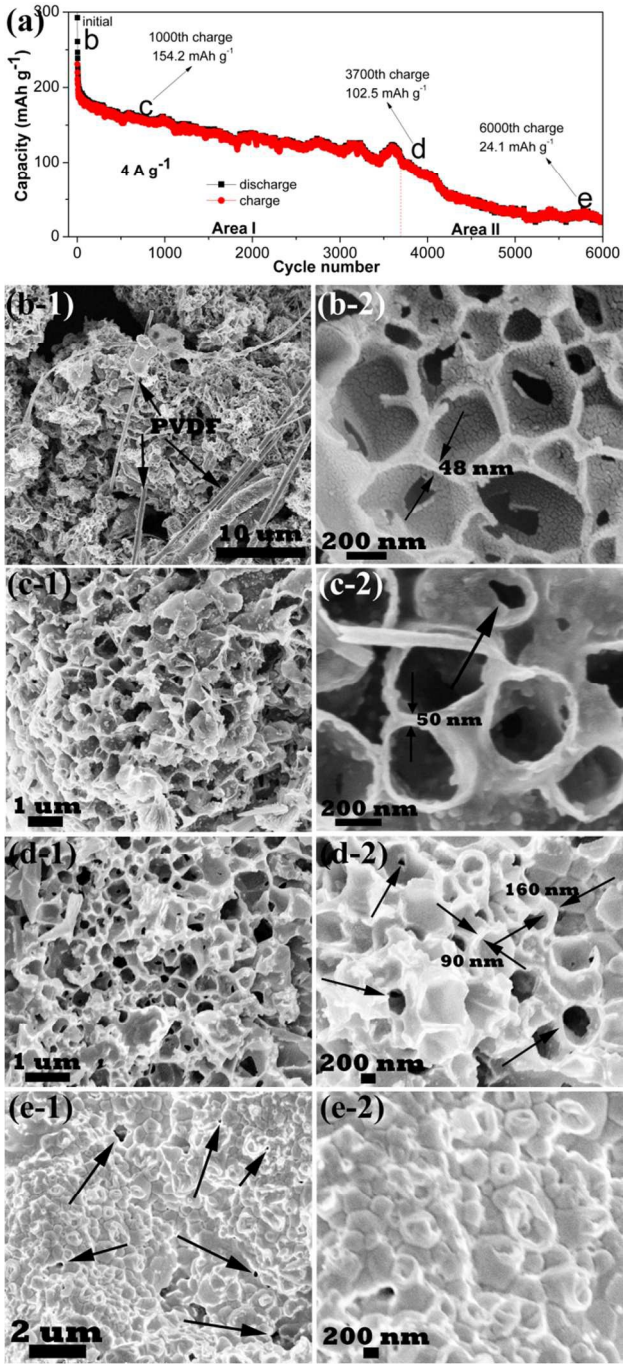

Figure 8 (a) Cycle performance of the 3DHCM electrode in 6,000 cycles at the current density of 4 A g^{-1}. (b), (c), (d), (e) SEM images of the cycled electrode ended at 0th, 1,000th, 3,700th and 6,000th charge.

231, 179.4, 158.3, 154.2, 140.6 and 138.1 mAh g^{-1} can be achieved. Even after 3,000 cycles, the comparable high reversible capacity of 116 mAh g^{-1} can still be obtained. To the best of our knowledge, this high rate behavior is unprecedented for a nonaqueous room temperature SIB anode.[4, 17, 28, 29, 32, 33, 41] The superior rate performance and ultralong cycle life described herein can be explained by the unique 3D porous nanostructure. The introduction of the porosity (macropores and mesopores) in effect reduces the sodium ion diffusion distances since the

electrolyte will be able to penetrate into the pores. The large surface area leads to a sufficiently large electrode/electrolyte interface to absorb sodium ions and promote rapid charge-transfer reactions.[45] At the same time, solid-state diffusion of ions has been proved to be the limiting factor for the high rate performance of bulk intercalation electrodes.[2, 46] The distances of sodium ion diffusion in 3DHCM are at the maximum of half of those thicknesses, only ranging from 2.5 to 15 nm (Figure 2). Based on Fick's first law, the diffusion time is proportional to the diffusion distance squared, if all else being equal, thinner walls of carbon would sodiate faster. In addition, the 3D porous matrix not only acts as reservoirs for storage of sodium ions, but also accommodates the local volume change of the carbon anode material, leading to the integrity of the porous structure and further ultralong cycle life of the electrode.

To further study the cycle stability of the 3DHCM electrode, the ex-situ SEM was performed on the cycled electrodes at different charging end states in the electrochemical process (Noting that the different charging end states were from different half-cells, these different half-cells delivered nearly identical cycle performance in 6,000 cycles). Figure 8a displays the cycle performance of the 3DHCM electrode in 6,000 cycles at the current density of 4 A g^{-1}. 3,700th cycle is a watershed in the whole cycles. Before 3,700th cycle (Area I), the reversible capacities are slowly decaying with the average rate of 0.014 mAh g^{-1} per cycle; while the decaying rate increases to more than 0.034 mAh g^{-1} per cycle after 3,700 cycles(Area II). Good cycle stability is derived from the porous structure maintaining. Before 1000th cycles, the 3D porous structure can be well maintained with legible macropores and pore walls (Figure 8b-1, -2 and 8c-1, -2). A uniform SEI film was generated in the pores and between the pores with some pores shrinking, shown in Figure 8c-2. At 3,700th charging end state, many pores shrink further and even are blocked up with the thickness of pore walls increasing maybe due to the further decomposition of the electrolyte (1 M $NaClO_4$ in PC) and/or the accumulation of sodium plating at high rate (Figure 8d-1, -2).[29] The thick pore walls and clogged macropores lead to internal carbon inactivation and increase dramatically the diffusion paths of sodium ions, resulting in the capacity fading and poor rate performance of the electrode in subsequent cycles. Figure 8e-1, -2 deliver the SEM images of the electrode ended at 6000th charge. The macropores in 3DHCM disappear and the final reversible charge capacity is only 24.1 mAh g^{-1}. The result of ex-situ SEM images further confirms that the 3D porous structure is of importance to the ultralong cycle life of the 3DHCM electrode.

A sodium-ion full cell is also demonstrated using 3-D hard carbon matrix as anode and $Na_3V_2(PO_4)_3$/C[47] as cathode. Figure 9a shows the front two discharge/charge curves of $Na_3V_2(PO_4)_3$/C at a current rate of C/10 (59 mA g^{-1}) in the voltage range of 2.5 and 3.8 V vs. Na^+/Na. The voltage profile has flat charge and discharge plateaus at about 3.45 and 3.30 V, showing the initial discharge capacity of 107 mAh g^{-1}. Up to 300th cycle, the 83.7 mAh g^{-1} of charge capacity and discharge capacity of 82.1 mAh g^{-1} can be obtained at the current rate of 1C (Figure 9b). Figure 9c shows 1st, 5th and 50th discharge/charge profiles of 3DHCM ‖ $Na_3V_2(PO_4)_3$/C sodium-ion full cell at the current density of 500 mA g^{-1} between 0.5 and 3.5 V. The first charge and discharge capacities are 198.6 and 115.6 mAh g^{-1}, respectively, with large irreversible discharge capacity loss due to the low initial coulombic efficiency of 3DHCM anode at the current density of 500 mA g^{-1}. Preliminary results show that the full cell gives rise to the average charge and discharge voltages at ca. 2.2 and 1.6 V, respectively. It can be seen that a reversible capacity of about 90 mAh g^{-1} can be achieved till to 50th cycles. However, the capacities decay dramatically in the subsequent cycles. The full-cell performance can be further enhanced by optimization of both electrodes and their weight ratio. At the same time, XRD pattern of the cycled cathode electrode (Figure 9d) indicates that the crystal structure of $Na_3V_2(PO_4)_3$/C is not be changed. The study of the sodium-ion full cell is going on, especially the optimization of the performances.

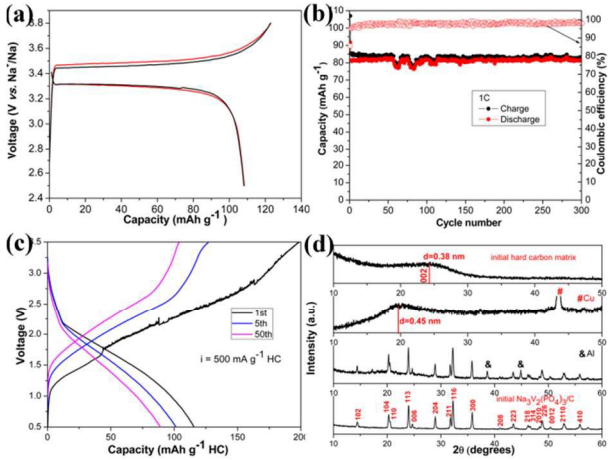

Figure 9 (a) The front two discharge/charge curves of $Na_3V_2(PO_4)_3$/C at a current rate of C/2 (59 mA g^{-1}) in the voltage range of 2.5 and 3.8 V vs. Na^+/Na. (b) Cycle performance of $Na_3V_2(PO_4)_3$/C at a current rate of 1C in the voltage range of 2.5 and 3.8 V vs. Na^+/Na. (c) The 1st, 5th and 50th discharge/charge profiles of 3DHCM ‖ $Na_3V_2(PO_4)_3$/C sodium-ion full cell at the current density of 500 mA g^{-1} between 0.5 and 3.5 V. (d) XRD patterns of the cycled cathode/anode electrodes after 50 cycles at 500 mA g^{-1}.

Conclusions

In this study we synthesized and tested a three-dimensional (3D) hard carbon matrix (3DHCM) derived from sodium polyacrylate precursor. Taking the advantage of the special molecular structure of sodium polyacrylate, we achieved a porous structure composed of very thin interconnected carbon nanosheets with a highly dilated graphene interlayer spacing. Unique 3-D open structural features endow the 3DHCM with superior SIB performance, that is, a superior rate performance and ultralong cycle life (116 mAh g^{-1} can be achieved after 3,000 cycles at 4 A g^{-1}). The introduction of the stable porosity effectively reduces the sodium ion diffusion distances since the electrolyte will be able to completely penetrate into the pores. At the same time, the very short sodium ions diffusion distances in the thin carbon nanosheets further facilitate the fast sodium-ion extraction/insertion. More obvious “graphitic” domains are self-produced and detected for the first time in the electrochemical sodium ions insertion/extraction, which leads to the trend of the sloping capacity percentage increasing in total discharge. The electrolyte severely decomposed on the electrode/electrolyte

interface in the deep electrochemical cycles, resulting in fast capacity fading. In addition, a sodium-ion full cell is also demonstrated using 3-D hard carbon matrix as anode. The results demonstrate that the 3DHCM are a promising candidate for the construction of low-cost sodium ion battery systems that perform on a competitive level with Li-ion systems. We believe that these findings obtained here not only deepen the understanding of the electrochemical process for hard carbon, but also open a new avenue in the search of even better and low cost negative electrode materials and will be helpful in speeding up the development of room-temperature long-life sodium-ion batteries for large-scale energy storage systems.

Notes and references

[a] *College of Physical and Electronic Engineering, Changshu Institute of Technology, China; E-mail: yuanzhengqiu@yahoo.com;yuanzhengqiu@gmail.com.*
[b] *Department of Chemistry, University of Science and Technology of China, China*

† Electronic Supplementary Information (ESI) available: more HRTEM images and EDS for the electrode after 100th charge, and charge-discharge curves at different current densities. See DOI: 10.1039/b000000x/

1 J. M. Tarascon, *Nat. Chem.*, 2010, **2**, 510.
2 N. Yabuuchi, M. Kajiyama, J. Iwatate, H. Nishikawa, S. Hitomi, R. Okuyama, R. Usui, Y. Yamada and S. Komaba, *Nat. Mater.*, 2012, **11**, 512.
3 J. F. Qian, M. Zhou, Y. L. Cao, X. P. Ai and H. X. Yang, *Adv. Energy Mater.*, 2012, **2**, 410.
4 V. Palomares, P. Serras, I. Villaluenga, K. B. Hueso, J. Carretero-Gonzalez and T. Rojo, *Energy Environ. Sci.*, 2012, **5**, 5884.
5 C. D. Wessells, M. T. McDowell, S. V. Peddada, M. Pasta, R. A. Huggins and Y. Cui, *ACS Nano*, 2012, **6**, 1688.
6 R. Berthelot, D. Carlier and C. Delmas, *Nat. Mater.*, 2011, **10**, 74.
7 Y. L. Cao, L. F. Xiao, W. Wang, D. W. Choi, Z. M. Nie, J. G. Yu, L. V. Saraf, Z. G. Yang and J. Liu, *Adv. Mater.*, 2011, **23**, 3155.
8 J. J. Ding, Y. N. Zhou, Q. Sun and Z. W. Fu, *Electrochem. Commun.*, 2012, **22**, 85.
9 H. M. Liu, H. S. Zhou, L. P. Chen, Z. F. Tang and W. S. Yang, *J. Power Sources*, 2011, **196**, 814.
10 S. Komaba, N. Yabuuchi, T. Nakayama, A. Ogata, T. Ishikawa and I. Nakai, *Inorg. Chem.*, 2012, **51**, 6211.
11 D. Carlier, J. H. Cheng, R. Berthelot, M. Guignard, M. Yoncheva, R. Stoyanova, J. Hwang and C. Delmasa, *Dalton Trans.*, 2011, **40**, 9306.
12 M. Sathiya, K. Hemalatha, K. Ramesha, J. M. Tarascon and A. S. Prakash, *Chem. Mater.*, 2012, **24**, 1846.
13 S. M. Oh, S. T. Myung, J. Hassoun, B. Scrosat and Y. K. Sun, *Electrochem. Commun.*, 2012, **14**, 149.
14 Z. Yuan, D. Wei, Y. Wang, Y. Zhu, Y. Qian and K. Tang, *CrystEngComm*, 2012, **14**, 4251.
15 H. T. Zhuo, X. Y. Wang, A. P. Tang, Z. M. Liu, S. Gamboa and P. J. Sebastian, *J. Power Sources,* 2006, **160**, 698.
16 Z. Jian, W. Han, X. Lu, H. Yang, Y.-S. Hu, J. Zhou , Z. Zhou, J. Li, W. Chen, D. Chen and L. Chen, *Adv. Energy Mater.*, 2013, **3**, 156.
17 J. Billaud, G. Singh, A. R. Armstrong, E. Gonzalo, V. Roddatis, M. Armand, T. Rojo and P. G. Bruce, *Energy Environ. Sci.*, 2014, **7**, 1387.
18 K. Saravanan , C. W. Mason , A. Rudola , K. H. Wong and P. Balaya, *Adv. Energy Mater.*, 2013, **3**, 444.
19 C. Zhu, K. Song, P. A. van Aken, J. Maier and Y. Yu, *Nano Lett.*, 2014, **14**, 2175.
20 J. Sangster, *J. Phase Equilib. Diffus.*, 2007, **28**, 571.
21 P. Senguttuvan, G. Rousse, V. Seznec, J. M. Tarascon and M. R. Palacin, *Chem. Mater.*, 2011, **23**, 4109.
22 Q. Sun, Q. Q. Ren, H. Li and Z. W. Fu, *Electrochem. Commun.*, 2011, **13**, 1462.
23 J. F. Qian, *Chem. Commun.*, 2012, **48**, 7070.
24 L. F. Xiao, *Chem. Commun.*, 2012, **48**, 3321.
25 Y. Wang, X. Yu, S. Xu, J. Bai, R. Xiao, Y.-S. Hu, H. Li, X.-Q. Yang, L. Chen and X. Huang, *Nat. Commun,*. 2013, **4**, 2365.
26 M. M. Doeff, Y. Ma, S. J. Visco and L. C. De Jonghe, *J. Electrochem. Soc.*, 1993, **140**, L169.
27 D. A. Stevens and J. R. Dahn, *J. Electrochem. Soc.*, 2000, **147**, 1271.
28 Z. Wang, L. Qie, L. Yuan, W. Zhang, X. Hu and Y. Huang, *Carbon*, 2013, **55**, 328.
29 S. Komaba, W. Murata, T. Ishikawa, N. Yabuuchi, T. Ozeki, T. Nakayama, A. Ogata, K. Gotoh and K. Fujiwara, *Adv. Funct. Mater.*, 2011, **21**, 3859.
30 Y. Cao, L. Xiao, M. L. Sushko, W. Wang, B. Schwenzer, J. Xiao, Z. Nie, L. V. Saraf, Z. Yang and J. Liu, *Nano Lett.*, 2012, **12**, 3783.
31 K. Tang, L. Fu, R. J. White, L. Yu, M. M. Titirici, M. Antonietti and J. Maier, *Adv. Energy Mater.*, 2012, **2**, 873.
32 J. Ding, H. Wang, Z. Li, A. Kohandehghan, K. Cui, Z. Xu, B. Zahiri, X. Tan, E. M. Lotfabad, B. C. Olsen and D. Mitlin, *ACS Nano*, 2013, **12**, 11004.
33 W. Li, L. Zeng, Z. Yang, L. Gu, J. Wang, X. Liu, J. Cheng and Y. Yu, *Nanoscale*, 2014, **6**, 693.
34 J. Zhao, L. Zhao, K. Chihara, S. Okada, J. Yamaki, S. Matsumoto, S. Kuze and K. Nakane, *J. Power Sources*, 2013, **244**, 752.
35 C. R. Perez, S. H. Yeon, J. Segalini, V. Presser, P. L. Taberna, P. Simon and Y. Gogotsi, *Adv. Funct. Mater.*, 2013, **23**, 1081.
36 J. T. Zhang and X. S. Zhao, *ChemSusChem*, 2012, **5**, 818.
37 J. R. Dahn, T. Zheng, Y. H. Liu and J. S. Xue, *Science*, 1995, **270**, 590.
38 D. Lozano-Castello´, M. A. Lillo-Ro´denas, D. Cazorla-Amoro´s and A. Linares-Solano, *Carbon*, 2001, **39**, 741.
39 C. Kim, K. S. Yang, M. Kojima, K. Yoshida, Y. J. Kim, Y. A. Kim and M. Endo, *Adv. Funct. Mater.*, 2006, **16**, 2393.
40 M. H. Gass, U. Bangert, A. L. Bleloch, P. Wang, R. R. Nair and A. K. Geim, *Nat. Nanotechnol.*, 2008, **3**, 676.
41 H. Wang, Z. Wu, F. Meng, D. Ma, X. Huang, L. Wang, and X. Zhang, *ChemSusChem*, 2013, **6**, 56.
42 Y. L. Cao, L. F. Xiao, X. P. Ai and H. X. Yang, *Electrochem. Solid-State Lett.*, 2003, **6**, A30.
43 D. A. Stevens and J. R. Dahn, *J. Electrochem. Soc.*, 2001, **148**, A803.
44 P. Thomas and D. Billaud, *Electrochim. Acta*, 2001, **46**, 3359.
45 J. H. Liu and X. W. Liu, *Adv. Mater.*, 2012, **24**, 4097.
46 Y. Shao, J. Xiao, W. Wang, M. Engelhard, X. Chen, Z. Nie, M. Gu, L. Saraf, G. Exarhos and J. Zhang, *Nano Lett.*, 2013, **8**, 3909.
47 L. Si, Z. Yuan, L. Hu, Y. Zhu and Y. Qian, *J. Power Sources.,* 2014, **272**, 880.